

Sloshing in a vertical circular cylindrical tank with an annular baffle. Part 2. Nonlinear resonant waves

I. Gavriluk · I. Lukovsky · Yu. Trotsenko ·
A. Timokha

Received: 23 May 2005 / Accepted: 4 July 2006 / Published online: 28 September 2006
© Springer Science+Business Media B.V. 2006

Abstract Weakly nonlinear resonant sloshing in a circular cylindrical baffled tank with a fairly deep fluid depth (depth/radius ratio ≥ 1) is examined by using an asymptotic modal method, which is based on the Moiseev asymptotic ordering. The method generates a nonlinear asymptotic modal system coupling the time-dependent displacements of the linear natural modes. Emphasis is placed on quantifying the effective frequency domains of the steady-state resonant waves occurring due to lateral harmonic excitations, versus the size and the location of the baffle. The forthcoming Part 3 will focus on the vorticity stress at the sharp baffle edge and related generalisations of the present nonlinear modal system.

Keywords Nonlinear sloshing · Modal system · Steady-state resonant waves

1 Introduction

Baffles are extensively used in various industrial applications to suppress sloshing, modify dynamic features of the coupled ‘fluid-structure’ mechanical systems and/or to increase the overall structural damping. When structural vibrations do not excite the lowest natural sloshing frequency, hydrodynamic loads owing to sloshing can often be quantified within the framework of a linear theory. The linear sloshing analysis was carried out in Part 1 [1]. Closeness of the lowest natural sloshing frequency to a control structural frequency leads to violent resonant fluid motions. As long as the ‘resonance’ structural vibrations are of relatively large magnitude and/or the liquid is shallow, these motions become strongly dissipative. Breaking

I. Gavriluk
Berufsakademie Thüringen-Staatliche Studienakademie,
Am Wartenberg 2, D-99817, Eisenach, Germany

I. Lukovsky · Yu. Trotsenko
Institute of Mathematics National Academy of Sciences of Ukraine,
Tereschenkivska 3, 01601, Kiev, Ukraine

A. Timokha (✉)
Centre for Ships and Ocean Structures,
Norwegian University of Science and Technology,
NO-7491, Trondheim, Norway
e-mail: alextim@marin.ntnu.no

waves and slamming may matter. Besides, baffles can penetrate the free surface and cause its fragmentation. Analytical investigations are then hardly possible. The interested engineers should look for specific numerical tools [2–5].

Sloshing is of a *weakly nonlinear nature* for *small-magnitude resonant excitations and a fairly deep fluid depth*. This is relevant to spacecraft applications and Tuned Sloshing Dampers. Fundamental studies by NASA [6], as well as experimental and numerical works by Bogoryad and Druzhinina [7], Mikishev [8], Mikishev and Churilov [9], showed that, even though flow separation occurs in a neighbourhood of the sharp baffle edge, the weakly nonlinear sloshing is satisfactorily predicted by an inviscid solution with irrotational flow. This solution constitutes an ‘ambient flow’. As shown by Cole [6], Buzhinskii [10] and Isaacson and Premasiri [11], using the inviscid solution also makes it possible to estimate the vortex shedding and related damping. Damping plays a secondary role in a qualitative description of the resonant steady-state sloshing. However, it considerably influences the transient waves. This conclusion follows from studies by Miles [12, 13] and Faltinsen et al. [14], who manipulated with a speculative increase/decrease of the damping rates.

Using the inviscid hydrodynamic model extends the number of suitable computational-fluid-dynamics (CFD) methods, which are applicable to weakly nonlinear baffled sloshing (see, the recent publications [15–19]). These methods are typically based on the finite-element technique. To the authors’ knowledge, the present paper is a pioneering work generalising a semi-analytical, *nonlinear multi-modal method* for baffled sloshing. Multi-modal methods have earlier been developed only for tanks without baffles [20–28].

Multi-modal methods use variational and asymptotic techniques to reduce the original free-boundary “sloshing” problem to a system of nonlinear ordinary differential equations (*modal system*). This makes it possible to consider sloshing as a mechanical system with a finite number of degrees of freedom. Each of its generalised coordinates is associated with a time-dependent coefficient in the Fourier representation of the free surface. The main advantages of multi-modal methods relative to traditional CFD-tools consist of (i) straightforward incorporation of modal systems into the dynamic equations of the whole object; this facilitates studies on coupled motions [27–30]; (ii) CPU-efficient simulations of both transient and steady-state weakly nonlinear waves [21, 23, 26, 31–33] and (iii) the possibility of analytical studies of steady-state (periodic) resonant waves in a harmonically oscillated tank [23–29, 34].

Because the steady-state resonant waves are realised on a long-time scale [25, 35, 36], task (iii) is tedious and CPU-demanding for CFD-methods. This is especially true for three-dimensional sloshing when several steady-state regimes co-exist for the same forcing parameters and irregular (‘chaotic’) motions may occur. In order to identify effective frequency domains of steady-state waves by direct simulations, an exhaustive search with various initial scenarios is required. Besides, CFD-methods may run into serious difficulties to distinguish hydrodynamic and numerical instabilities.

Hermann and Timokha [37] have categorised the multi-modal methods into the following four sub-classes: (I) Perko-like or pseudo-spectral methods [33, 38, 39], (II) the Miles–Lukovsky variational-asymptotic technique and its modifications [23, 29, 32, 40, 41], (III) modal methods based on separation of the quick and slow time scales [12, 13, 26, 42] (applicable only for harmonically forced tanks) and (IV) asymptotic modal methods, e.g. [27, 28], whose fundamentals are best represented by Narimanov [43, 44]. The usage of multi-modal methods needs analytically given natural sloshing modes. Moreover, even though the natural modes are theoretically defined only in the hydrostatic domain, the methods (I–III) require an extension of these modes through the unperturbed water plane to the actual time-varying flow domain. As a consequence, almost all the nonlinear modal systems have been derived for rectangular and circular-base tanks, i.e., when those analytical natural modes exist. Rare modal systems for some of complex shapes, e.g. [45] for a ∇ -shaped conical tank, are based on special approximations of the natural modes.

Part 1 constructs analytical approximate natural modes for a circular cylindrical tank with a rigid-ring baffle. These modes are given by a Green representation, which diverges outside the hydrostatic fluid shape. This means that these approximate modes are not defined in the time-varying flow domain and, therefore, the methods (I–III) cannot employ the results of Part 1. In contrast, although the original paper

by Narimanov [44] and existing modifications of his methods [44] also use the analytical natural modes that are expandable over the static fluid domain, this asymptotic technique may in general utilise the fundamental solutions from Part 1. There are two necessary conditions. First, the approximate natural modes should admit higher derivatives, whose projections on the water plane must belong to a suitable functional space. Second, the solution of Narimanov's recurrence boundary problems (computing higher-order asymptotic terms) must be presented as a Fourier series by approximate natural modes. The present paper demonstrates that the approximate natural modes of Part 1 satisfy these two conditions and derives the corresponding asymptotic modal system.

Furthermore, the paper concentrates on harmonic excitations of the lowest natural frequency. The third-order intermodal ordering by Moiseyev [46], following from the general theory of autonomous systems by Krylov-Bogoljubov [47] or a Duffing's analogy ([48, 49]), is used. The Moiseev asymptotics is common for the previous studies on resonant sloshing in a circular cylindrical tank without baffles [12, 13, 20, 21, 27–29, 44, 50]. It suggests that the scaled forcing amplitude $\epsilon \ll 1$ (ϵ is “excitation amplitude/radius” ratio) and the forcing frequency is close to the lowest natural frequency. A consequence is that the two lowest modes are of the dominating order $O(\epsilon^{1/3})$, but there exist an infinite number of $O(\epsilon^{2/3})$ -order modes. When studying resonant sloshing in a circular cylindrical tank without baffles, Miles [12, 13] has theoretically shown that the second-order contribution can be described precisely by only three second-order modes from this infinite set. Exceptions are associated with a critical fluid depth, for which internal (secondary) resonance occurs. Specific physical and geometrical argumentations for this result are given in [27, 28, 44]. Numerical results based on a five-mode approximation (two dominating and three second-order modes) agree with experiments [20–22, 27, 28]. The five-mode solution will be adopted in the present paper.

After a general statement of the problem in Sect. 2.1, Sect. 2.2 gives preliminaries from Part 1. In Sects. 2.3 and 2.4, the Narimanov method is used to derive a system of ordinary differential equations (modal system) governing time-dependent displacements of the five lowest natural modes. Argumentations by Miles [12, 13], Lukovsky [20], Gavriluk et al. [21], Ikeda and Murakami [27], Ikeda and Ibrahim [28] on the five-mode approximation for a smooth circular cylindrical tank are discussed. Section 2.5 includes an estimate of the secondary resonance and occurrence of shallow fluid flows. In Sect. 3, we study steady-state resonant sloshing.

In summary, the main results consist of (A) derivation of an asymptotic modal system for baffled sloshing (first in the literature); (B) study of steady-state nonlinear baffled sloshing; we show that there exist only ‘planar’ and ‘swirling’ resonant regimes, (C) estimate of effective frequency domains for steady-state regimes versus the size and the vertical location of the annular baffle.

2 Nonlinear multi-modal theory

2.1 Free-boundary problem

Let a rigid circular-base cylindrical tank of radius R_1 be partially filled by a fluid with mean depth h . The inner periphery of the tank is equipped with a thin rigid-ring baffle which divides h into h_1 and h_2 , where h_1 is the mean height of the fluid layer over the baffle. The thickness of the baffle is neglected. The radius of the circular hole is a (see, Fig. 1). The fluid sloshing is described within the framework of an inviscid hydrodynamic model with irrotational flow. It is assumed that the free surface $\Sigma(t)$ does not touch (cross) the baffle Γ . The problem is studied in the scaled formulation suggesting that all the lengths and physical constants are normalised by R_1 . This implies, in particular, that $h_1 := h_1/R_1$, $h_2 := h_2/R_1$, $g := g/R_1$ (gravity acceleration g has the dimension [s^{-2}]), etc. The free-boundary problem is formulated in the tank-fixed coordinate system $Oxyz$. The non-dimensional h_1 and h_2 are assumed to be finite. Shallow-water waves are not considered.

Without loss of generality, the Oz -axis is directed along the symmetry axis and the origin O is posed on the baffle plane as shown in Fig. 1. Furthermore, the analysis is restricted to prescribed translatory tank oscillations, which are governed by the time-dependent vector $\mathbf{v}_O(t) = (v_{O1}(t), v_{O2}(t), v_{O3}(t))^T$ (translatory velocity of the mobile coordinate system relative to an absolute coordinate system $O'x'y'z'$).

The free-boundary-value problem takes the following form (see [29, 51, 52]):

$$\left. \begin{aligned} \Delta\Phi &= 0 \quad \text{in } Q(t); \quad \frac{\partial\Phi}{\partial\nu} = \mathbf{v}_O \cdot \boldsymbol{\nu} \quad \text{on } S(t) \cup \Gamma, \\ \frac{\partial\Phi}{\partial\nu} &= \mathbf{v}_O \cdot \boldsymbol{\nu} + \frac{f_t}{\sqrt{1+(\nabla f)^2}} \quad \text{on } \Sigma(t); \quad \int_{Q(t)} dQ = \text{const}, \\ \frac{\partial\Phi}{\partial t} + \frac{1}{2}(\nabla\Phi)^2 - \nabla\Phi \cdot \mathbf{v}_O + gf &= 0 \quad \text{on } \Sigma(t). \end{aligned} \right\} \quad (1)$$

Here, the unknowns are $f(x, y, t)$ defining the free surface $\Sigma(t): z = f(x, y, t)$ and the absolute velocity potential $\Phi(x, y, z, t)$, which is defined in the time-varying $Q(t)$. The latter is confined to the wetted body surface $S(t)$, the baffle surface Γ and $\Sigma(t)$, $\boldsymbol{\nu}$ is the outward normal vector.

Assuming a resonant lateral harmonic excitation implies

$$v_{O1}(t) = -\sigma\epsilon \sin \sigma t; \quad v_{O2} = v_{O3} \equiv 0. \quad (2)$$

Here $\epsilon \ll 1$ is the non-dimensional amplitude and $\sigma \rightarrow \omega_1^{(1)}$, where $\omega_1^{(1)}$ is the lowest natural sloshing frequency.

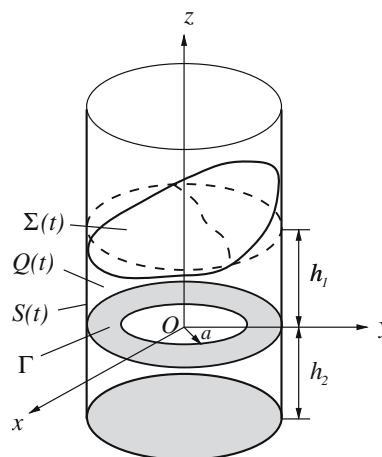
The free-boundary problem (1) should be completed by either initial or periodicity conditions. The initial (Cauchy) conditions assume

$$f(x, y, t_0) = f_0(x, y); \quad \frac{\partial\Phi}{\partial\nu} \Big|_{z=f_0(x,y)} = \Phi_0(x, y, z) \quad (3)$$

to be known at $t = t_0$. The steady-state harmonic solutions are associated with the $T = 2\pi/\sigma$ -periodic wave patterns, i.e.,

$$f(x, y, t + T) = f(x, y, t); \quad \nabla\Phi(x, y, z, t + T) = \nabla\Phi(x, y, z, t). \quad (4)$$

Fig. 1 Sketch of a baffled circular cylindrical tank partially filled by a fluid



2.2 Preliminaries from Part 1

Part 1 concentrated on the natural sloshing modes. These are associated with eigenfunctions of the following spectral problem

$$\left. \begin{aligned} \Delta\varphi = 0 \quad \text{in } Q_0; \quad \frac{\partial\varphi}{\partial\nu} = 0 \quad \text{on } S_0 \text{ and } \Gamma, \\ \frac{\partial\varphi_i}{\partial z} = \kappa\varphi \quad \text{on } \Sigma_0; \quad \int_{\Sigma_0} \varphi \, dS = 0 \end{aligned} \right\} \tag{5}$$

with the spectral parameter κ on the unperturbed (hydrostatic) water plane Σ_0 (see, geometric definitions in Fig. 2a).

The spectral problem (5) has the real positive eigenvalues. Its eigenfunctions satisfy the zero Neumann boundary condition on $S_0 + \Gamma$, but projections of the eigenfunctions on Σ_0 constitute a basis in $L_2(\Sigma_0)$. By separating the spatial variables in the (r, θ, z) cylindrical coordinate system ($x = r \cos \theta, y = r \sin \theta, z = z$) and introducing

$$\varphi(r, \theta, z) = \psi^{(m)}(z, r) \exp(im\theta), \quad m = 0, 1, \dots; \quad i^2 = -1,$$

we reduced problem (5) to an m -parametric family of two-dimensional spectral problems in the meridional cross-section G (see, Fig. 2b).

Part 1 uses the domain decomposition

$$\psi^{(m)}(z, r) = \begin{cases} \psi^{(m,1)}(z, r), & \text{in } G_1, \\ \psi^{(m,2)}(z, r), & \text{in } G_2 \end{cases} \tag{6}$$

and derives the Green representation for each of the sub-domains as

$$\psi^{(m,1)}(z, r) = - \int_0^a N_m^{\kappa^{(m)}}(r_0) K_m^{\kappa^{(m)}}(z, r; r_0) r_0 dr_0, \quad \text{in } G_1, \tag{7}$$

$$\psi^{(m,2)}(z, r) = \int_0^a N_m^{\kappa^{(m)}}(r_0) K_m(z, r; r_0) r_0 dr_0 - \delta_{0m}, \quad \text{in } G_2. \tag{8}$$

Here δ_{im} is the Kronecker delta, $\kappa^{(m)}$ is an eigenvalue for the corresponding spectral problem in the meridional cross-section G , the kernels $K_m^{\kappa^{(m)}}$ and K_m are explicitly given by series in Bessel functions

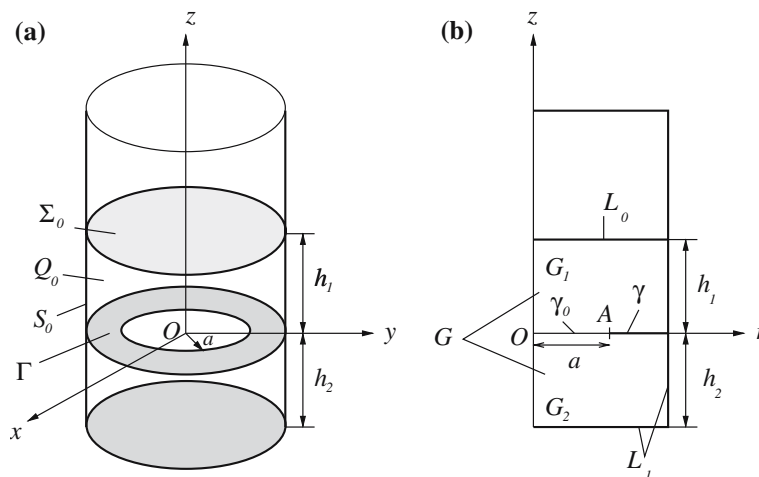


Fig. 2 Hydrostatic fluid shape in the baffled tank, three-dimensional and meridional sketches

and

$$N_m^{\kappa(m)}(r_0) = \frac{\partial \psi^{(m)}}{\partial z} \Big|_{z=0}, \quad 0 < r_0 < a.$$

The Dirichlet transmission condition on γ_0 yields a $\kappa^{(m)}$ -parametric integral equation with respect to $N_m^{\kappa(m)}$. Both the eigenvalues $\kappa_i^{(m)}$ and the corresponding $N_m^{\kappa_i^{(m)}}$, $m = 0, 1, \dots$; $i = 1, 2, \dots$ are found from this integral equation by a Galerkin method. A special functional basis reflects the singular behaviour of $N_m^{\kappa_i^{(m)}}$ at the sharp edges (as $r_0 \rightarrow a$). The method demonstrates fast convergence and high precision.

2.3 Nonlinear asymptotic modal system

As remarked in the Introduction, there exist four sub-classes of multi-modal methods. In common, these methods utilise a Fourier representation of the free surface by projections of the natural modes on Σ_0 . This reads

$$f(r, \theta, t) = \sum_{m=0}^{\infty} \sum_{i=1}^{\infty} (\beta_{m,i}^s(t) \sin \theta + \beta_{m,i}^c(t) \cos \theta) \tilde{F}_i^{(m)}(r) \quad (9)$$

in the cylindrical coordinate system $Or\theta z$. Here, $\beta_{m,i}^s(t)$ and $\beta_{m,i}^c(t)$ are time-dependent (modal) functions and $\tilde{F}_i^{(m)}(r)$ are the normalised radial profiles of the natural modes (see, the non-normalised definition in Equation (13) of Part 1) as follows

$$\tilde{F}_i^{(m)}(r) = \frac{\psi_i^{(m,1)}(h_1, r)}{\psi_i^{(m,1)}(h_1, 1)}, \quad 0 < r < 1, \quad m = 0, \dots; \quad i = 1, \dots$$

so that

$$\eta_{\max} = \max_{0 \leq \theta < 2\pi} \sum_{m=0}^{\infty} \sum_{i=1}^{\infty} (\beta_{m,i}^s(t) \sin \theta + \beta_{m,i}^c(t) \cos \theta)$$

implies a maximum instant wave elevation at the upright walls.

Multi-modal methods also need an analogous modal representation for the velocity potential Φ . The Introduction mentions the three most popular sub-classes of multi-modal methods, which are based on a Fourier series of the natural modes. These require that the eigenfunctions of (5) are analytically defined, not only in Q_0 , but also in the time-dependent fluid domain $Q(t)$. Because the kernels in (7)–(8) diverge over Σ_0 , these methods cannot use results of Part 1 to derive a nonlinear modal system. That is why the paper adopts the asymptotic method by Narimanov. It may employ (7)–(8).

Narimanov et al. [44] gave all the formal formulas of his asymptotic scheme for an arbitrarily shaped tank. However, to the author's knowledge, his method has been elaborated only for circular and rectangular-base tanks without baffles. A reason may be the difficulties involved in constructing approximate natural modes, which provide convergence to the coefficients of the corresponding modal system. The solutions (7)–(8) allow for that, at least, for a subset of a, h_1 and h_2 . This is shown in the Appendix.

In order to derive a system of ordinary differential equations (modal system) coupling $\{\tilde{\beta}_{m,i}(t)\} = \{\beta_{m,i}^s(t)\} \cup \{\beta_{m,i}^c(t)\}$, Narimanov [43, 44] proposed the following expression for the velocity potential

$$\Phi(r, \theta, z, t) = -r\sigma\epsilon \cos(\theta) \sin(\sigma t) + \sum_{m=0}^{\infty} \sum_{i=1}^{\infty} \left(\frac{d\beta_{m,i}^s(t)}{dt} \phi_i^{(m,s)}(r, \theta, z, t) + \frac{d\beta_{m,i}^c(t)}{dt} \phi_i^{(m,c)}(r, \theta, z, t) \right). \quad (10)$$

This expression follows from linear sloshing theory. One can see that the linearisation makes $\phi_i^{(m,s)}$ and $\phi_i^{(m,c)}$ to coincide with the natural modes $\sin(m\theta) \psi_i^{(m)}(z, r)$ and $\cos(m\theta) \psi_i^{(m)}(z, r)$, respectively. Further,

inserting (9), (10) into (1) establishes that $\phi_F = (\phi_i^{(m,s)}$ or $\phi_i^{(m,c)})$ is a solution of the following Neumann boundary-value problem

$$\Delta\phi_F = 0 \quad \text{in } Q(t); \quad \frac{\partial\phi_F}{\partial\nu} = 0 \quad \text{on } S(t) \text{ and } \Gamma,$$

$$\frac{\partial\phi_F}{\partial\nu} = \frac{F(r, \theta)}{\sqrt{1 + (\nabla f)^2}} \quad \text{on } \Sigma(t), \tag{11}$$

where $F(r, \theta)$ coincides with $\tilde{F}_i^{(m)}(r) \sin(m\theta)$ or $\tilde{F}_i^{(m)}(r) \cos(m\theta)$, respectively. The functions $\phi_i^{(m,s)}$ and $\phi_i^{(m,c)}$ parametrically depend on $\tilde{\beta}_{m,i}$. If deviations of the free surface $\Sigma(t): z = f(r, \theta, t)$ are small, the solution of (11) permits a Taylor expansion by $\tilde{\beta}_{m,i}$:

$$\phi_F(r, \theta, z, t) = \phi_F^{(0)}(r, \theta, z) + \sum_{m=0}^{\infty} \sum_{i=1}^{\infty} \tilde{\beta}_{m,i} \phi_{F,mi}^{(1)}(r, \theta, z) + \sum_{m,n=0}^{\infty} \sum_{i,j=1}^{\infty} \tilde{\beta}_{m,i} \tilde{\beta}_{n,j} \phi_{F,mi,nj}^{(2)}(r, \theta, z) + \dots, \tag{12}$$

where $\phi_F^{(0)}(r, \theta, z)$, $\phi_{F,mi}^{(1)}(r, \theta, z)$, $\phi_{F,mi,nj}^{(2)}(r, \theta, z)$ etc. should be found from a set of recursive Neumann boundary-value problems in the hydrostatic domain Q_0 with zero (on S_0) and non-zero (on Σ_0) Neumann boundary conditions. For circular cylindrical tanks without baffles, a Bessel-function algebra can be used to find solutions of these boundary-value problems. In our case, $\phi_{F,mi}^{(1)}(r, \theta, z)$, $\phi_{F,mi,nj}^{(2)}(r, \theta, z)$, etc. should be found numerically as truncated Fourier series by $\phi_F^{(0)}(r, \theta, z)$. This is exemplified in the Appendix.

When assuming that we know $\phi_{F,mi}^{(1)}(r, \theta, z)$, $\phi_{F,mi,nj}^{(2)}(r, \theta, z)$, etc., substituting (9), (10) and (12) in the last boundary condition of (1), using a Taylor expansion by $\tilde{\beta}_{m,i}$ and implementing a projective procedure on Σ_0 (in terms of the basic functions $\{\tilde{F}_i^{(m)}(r) \sin(m\theta), \tilde{F}_i^{(m)}(r) \cos(m\theta)\}$) leads to a required infinite-dimensional system of ordinary differential equations coupling $\ddot{\tilde{\beta}}_{m,i}(t)$, $\dot{\tilde{\beta}}_{m,i}(t)$ and $\tilde{\beta}_{m,i}(t)$.

2.4 Asymptotic modal system for resonant sloshing due to lateral harmonic excitations (2)

As shown by Lukovsky [20] and Miles [13], resonant lateral harmonic excitation of the lowest natural modes in a circular cylindrical tank invertible yields a Duffing-like intermodal ordering. In our case, this implies

$$\beta_{1,1}^c \sim \beta_{1,1}^s = O(\epsilon^{1/3}), \quad \beta_{2,i}^c \sim \beta_{2,i}^s \sim \beta_{0,i}^c \sim \beta_{0,i}^s = O(\epsilon^{2/3}),$$

$$\beta_{j,i}^c \sim \beta_{j,i}^s \lesssim O(\epsilon), \quad j \geq 3, \quad i = 1, 2, \dots \tag{13}$$

Here, two modal functions $\beta_{1,1}^c$ and $\beta_{1,1}^s$ are dominating, but the infinite set $\beta_{2,i}^c, \beta_{2,i}^s, \beta_{0,i}^c, \beta_{0,i}^s, i = 1, 2, \dots$ is of second order relative to $\beta_{1,1}^c$ and $\beta_{1,1}^s$. The remaining modes contribute only $O(\epsilon)$ and, pursuing an approximation of the free surface to within $O(\epsilon)$, we can neglect them. Thus, the nonlinear modal systems based on (13) should have an infinite number of degrees of freedom.

Miles [12, 13] demonstrated that separating the slow and fast time scales makes it possible to derive a Hamiltonian system, which governs the dominating $O(\epsilon^{1/3})$ -amplitudes and accounts for the feedback formed by the second-order modes ($O(\epsilon)$ -modal functions do not affect $\beta_{1,1}^c$ and $\beta_{1,1}^s$). Further, he has shown that $\beta_{2,i}^c, \beta_{2,i}^s, \beta_{0,i}^c, \beta_{0,i}^s, i \geq 2$ contribute less than 1% to the fixed-point solutions (steady-state waves), unless the depth/radius ratio is close to the critical value 0.831 or shallow. The critical depth leads to a secondary resonance. Comparisons with experimental data done by Lukovsky [20], Gavriluk et al. [21], Ikeda and Murakami [27] and Ikeda and Ibrahim [28] have confirmed that the five-mode approximation associated with $\beta_{1,1}^c, \beta_{1,1}^s, \beta_{2,1}^c, \beta_{2,1}^s$ and $\beta_{0,1}^c$ gives good agreement with measurements of the wave elevations and hydrodynamic forces.

The approximate natural modes of Part 1 cannot be used in the method by Miles [12, 13]. The use of a large set of the second-order modes is also hardly possible in the Narimanov’s method. The reason is a

dramatical increase of numerical operations. However, conclusions by Miles and Lukovsky are definitely true for a small-size baffle and a small hole radius a . The first limit case can be considered as a perturbed solution by Miles. The second case is characterised by almost zero flux through the baffle hole and, as a consequence, baffled sloshing is mainly determined by the fluid flow in the upper subdomain ($z > 0$). We must, however, guarantee that the secondary resonance does not occur. This will be studied in the next subsection.

The usage of the following five-dimensional modal expression

$$f(r, \theta, t) = \beta_{0,1}^c(t) F_1^{(0)}(r) + \left[\beta_{1,1}^s(t) \sin \theta + \beta_{1,1}^c(t) \cos \theta \right] F_1^{(1)}(r) + \left[\beta_{2,1}^s(t) \sin 2\theta + \beta_{2,1}^c(t) \cos 2\theta \right] F_1^{(2)}(r), \quad (14)$$

in the Narimanov scheme and disregarding terms of $o(\epsilon)$ make it possible to derive the following system of nonlinear ordinary differential equations

$$\begin{aligned} & \ddot{\beta}_{1,1}^s + \omega_1^{(1)} \beta_{1,1}^s \\ & + D_1((\beta_{1,1}^s)^2 \ddot{\beta}_{1,1}^s + \beta_{1,1}^s (\dot{\beta}_{1,1}^s)^2 + \beta_{1,1}^s \beta_{1,1}^c \ddot{\beta}_{1,1}^c + \beta_{1,1}^s (\dot{\beta}_{1,1}^c)^2) \\ & + D_2((\beta_{1,1}^c)^2 \ddot{\beta}_{1,1}^s + 2\beta_{1,1}^c \dot{\beta}_{1,1}^s \dot{\beta}_{1,1}^c - \beta_{1,1}^s \beta_{1,1}^c \ddot{\beta}_{1,1}^c - 2\beta_{1,1}^s (\dot{\beta}_{1,1}^c)^2) \\ & - D_3(\beta_{2,1}^c \ddot{\beta}_{1,1}^s - \beta_{2,1}^s \ddot{\beta}_{1,1}^c + \dot{\beta}_{1,1}^s \dot{\beta}_{2,1}^c - \dot{\beta}_{1,1}^c \dot{\beta}_{2,1}^s) \\ & + D_4(\beta_{1,1}^s \ddot{\beta}_{2,1}^c - \beta_{1,1}^c \ddot{\beta}_{2,1}^s) + D_5(\beta_{0,1}^c \ddot{\beta}_{1,1}^s + \dot{\beta}_{1,1}^s \dot{\beta}_{0,1}^c) \\ & + D_6(\beta_{1,1}^s \ddot{\beta}_{0,1}^c) = 0, \end{aligned} \quad (15)$$

$$\begin{aligned} & \ddot{\beta}_{1,1}^c + \omega_1^{(1)} \beta_{1,1}^c \\ & + D_1((\beta_{1,1}^c)^2 \ddot{\beta}_{1,1}^c + \beta_{1,1}^s \beta_{1,1}^c \ddot{\beta}_{1,1}^s + \beta_{1,1}^c (\dot{\beta}_{1,1}^s)^2 + \beta_{1,1}^c (\dot{\beta}_{1,1}^c)^2) \\ & + D_2((\beta_{1,1}^s)^2 \ddot{\beta}_{1,1}^c - \beta_{1,1}^s \beta_{1,1}^c \ddot{\beta}_{1,1}^s + 2\beta_{1,1}^s \dot{\beta}_{1,1}^s \dot{\beta}_{1,1}^c - 2\beta_{1,1}^c (\dot{\beta}_{1,1}^s)^2) \\ & + D_3(\beta_{2,1}^c \ddot{\beta}_{1,1}^c + \beta_{2,1}^s \ddot{\beta}_{1,1}^s + \dot{\beta}_{1,1}^s \dot{\beta}_{2,1}^s + \dot{\beta}_{1,1}^c \dot{\beta}_{2,1}^c) \\ & - D_4(\beta_{1,1}^c \ddot{\beta}_{2,1}^c + \beta_{1,1}^s \ddot{\beta}_{2,1}^s) + D_5(\beta_{0,1}^c \ddot{\beta}_{1,1}^c + \dot{\beta}_{1,1}^c \dot{\beta}_{0,1}^c) \\ & + D_6(\beta_{1,1}^c \ddot{\beta}_{0,1}^c) - \Lambda \ddot{v}_{O1} = 0, \end{aligned} \quad (16)$$

$$\ddot{\beta}_{0,1}^c + \omega_1^{(0)} \beta_{0,1}^c + D_{10}(\beta_{1,1}^s \ddot{\beta}_{1,1}^s + \beta_{1,1}^c \ddot{\beta}_{1,1}^c) + D_8((\dot{\beta}_{1,1}^s)^2 + (\dot{\beta}_{1,1}^c)^2) = 0, \quad (17)$$

$$\ddot{\beta}_{2,1}^s + \omega_1^{(2)} \beta_{2,1}^s - D_9(\ddot{\beta}_{1,1}^s \beta_{1,1}^c + \ddot{\beta}_{1,1}^c \beta_{1,1}^s) - 2D_7(\dot{\beta}_{1,1}^s \dot{\beta}_{1,1}^c) = 0, \quad (18)$$

$$\ddot{\beta}_{2,1}^c + \omega_1^{(2)} \beta_{2,1}^c + D_9(\ddot{\beta}_{1,1}^s \beta_{1,1}^s - \ddot{\beta}_{1,1}^c \beta_{1,1}^c) + D_7((\dot{\beta}_{1,1}^s)^2 - (\dot{\beta}_{1,1}^c)^2) = 0, \quad (19)$$

where $\omega_i^{(m)} = \sqrt{g\kappa_i^{(m)}}$ and D_i , $i = 1, \dots, 10$; Λ are functions of h_1, h_2 and a computed by

$$\begin{aligned} D_1 &= \frac{d_1}{\mu_{11}}; \quad D_2 = \frac{d_2}{\mu_{11}}; \quad D_3 = \frac{d_3}{\mu_{11}}; \quad D_4 = \frac{d_4}{\mu_{11}}, \\ D_5 &= \frac{d_5}{\mu_{11}}; \quad D_6 = \frac{d_6}{\mu_{11}}; \quad D_7 = \frac{d_7}{\mu_{21}}; \quad D_8 = \frac{d_8}{\mu_{01}}, \\ D_9 &= \frac{d_4}{\mu_{21}}; \quad D_{10} = \frac{d_6}{\mu_{01}}; \quad \Lambda = \frac{\lambda}{\mu_{11}}, \end{aligned} \quad (20)$$

where expressions for d_i , $i = 1, \dots, 8$; $\mu_{11}, \mu_{01}, \mu_{21}$ are derived in the Appendix. Some of the values in Table 1 may be of interest to the reader.

Table 1 Coefficients in (21) versus h_1 and a ; $h_1 + h_2 = 1.0$

h_1	μ_{01}	μ_{11}	μ_{21}	$\kappa_1^{(0)}$	$\kappa_1^{(1)}$	$\kappa_1^{(2)}$	d_1	d_2	d_3	d_4	d_5	d_6	λ
Coefficients for $a = 0.4$													
0.25	1.0424	1.1096	0.4374	2.9084	0.9286	2.0076	3.6519	1.4384	0.8838	0.6474	1.7457	-0.8467	0.8971
0.30	0.9654	0.9961	0.3934	3.1778	1.0518	2.2471	2.3531	0.7392	0.8303	0.4236	1.5966	-0.5777	0.9041
0.35	0.9170	0.9140	0.3642	3.3738	1.1615	2.4383	1.6583	0.3697	0.7893	0.2839	1.4848	-0.4153	0.9095
0.40	0.8855	0.8524	0.3443	3.5136	1.2585	2.5881	1.2499	0.1569	0.7576	0.1909	1.3963	-0.3102	0.9138
0.45	0.8645	0.8048	0.3303	3.6120	1.3436	2.7038	0.9926	0.0263	0.7327	0.1262	1.3245	-0.2387	0.9170
0.50	0.8504	0.7673	0.3204	3.6805	1.4179	2.7921	0.8216	-0.0576	0.7128	0.0795	1.2656	-0.1881	0.9195
0.55	0.8408	0.7375	0.3132	3.7280	1.4822	2.8589	0.7031	-0.1135	0.6969	0.0451	1.2171	-0.1512	0.9214
0.60	0.8343	0.7134	0.3081	3.7607	1.5377	2.9091	0.6182	-0.1518	0.6839	0.0192	1.1770	-0.1235	0.9229
Coefficients for $a = 0.5$													
0.25	0.9699	0.9462	0.4106	2.9996	1.0445	2.0807	2.8393	0.9970	0.6863	0.4825	1.2082	-0.6779	0.8796
0.30	0.9199	0.8765	0.3759	3.2463	1.1588	2.3072	1.8781	0.5052	0.6965	0.3177	1.2251	-0.4677	0.8911
0.35	0.8883	0.8247	0.3526	3.4236	1.2582	2.4862	1.3578	0.2363	0.6963	0.2122	1.2223	-0.3394	0.9001
0.40	0.8674	0.7847	0.3365	3.5490	1.3445	2.6255	1.0490	0.0764	0.6916	0.1404	1.2079	-0.2556	0.9069
0.45	0.8531	0.7529	0.3251	3.6368	1.4193	2.7325	0.8527	-0.0245	0.6851	0.0893	1.1872	-0.1981	0.9121
0.50	0.8432	0.7271	0.3168	3.6978	1.4837	2.8139	0.7210	-0.0910	0.6780	0.0520	1.1642	-0.1572	0.9160
0.55	0.8362	0.7059	0.3108	3.7399	1.5391	2.8753	0.6289	-0.1363	0.6709	0.0241	1.1412	-0.1272	0.9190
0.60	0.8313	0.6885	0.3063	3.7689	1.5865	2.9214	0.5625	-0.1678	0.6644	0.0028	1.1196	-0.1047	0.9211
Coefficients for $a = 0.6$													
0.25	0.8811	0.7926	0.3721	3.1508	1.2039	2.2157	2.0178	0.5927	0.5571	0.3124	0.8822	-0.4784	0.8649
0.30	0.8639	0.7615	0.3505	3.3583	1.3024	2.4169	1.3823	0.2767	0.6014	0.2041	0.9804	-0.3360	0.8812
0.35	0.8530	0.7372	0.3356	3.5041	1.3855	2.5729	1.0363	0.0978	0.6258	0.1326	1.0365	-0.2478	0.8934
0.40	0.8450	0.7170	0.3250	3.6059	1.4560	2.6927	0.8298	-0.0120	0.6390	0.0826	1.0655	-0.1895	0.9025
0.45	0.8389	0.6999	0.3172	3.6765	1.5161	2.7839	0.6974	-0.0833	0.6454	0.0463	1.0773	-0.1490	0.9092
0.50	0.8341	0.6853	0.3113	3.7253	1.5672	2.8528	0.6079	-0.1314	0.6478	0.0192	1.0787	-0.1199	0.9141
0.55	0.8304	0.6726	0.3069	3.7589	1.6106	2.9046	0.5446	-0.1648	0.6477	-0.0013	1.0742	-0.0983	0.9177
0.60	0.8275	0.6617	0.3036	3.7819	1.6475	2.9433	0.4983	-0.1884	0.6463	-0.0170	1.0665	-0.0820	0.9203
Coefficients for $a = 0.7$													
0.25	0.8049	0.6764	0.3306	3.3580	1.3991	2.4266	1.2826	0.2531	0.5073	0.1603	0.7654	-0.2876	0.8615
0.30	0.8167	0.6728	0.3228	3.5071	1.4722	2.5837	0.9303	0.0724	0.5593	0.0982	0.8780	-0.2077	0.8805
0.35	0.8233	0.6678	0.3168	3.6091	1.5321	2.7023	0.7391	-0.0331	0.5912	0.0558	0.9476	-0.1574	0.8940
0.40	0.8260	0.6619	0.3120	3.6791	1.5819	2.7918	0.6246	-0.0998	0.6107	0.0252	0.9889	-0.1235	0.9036
0.45	0.8266	0.6556	0.3081	3.7272	1.6237	2.8589	0.5504	-0.1440	0.6223	0.0026	1.0118	-0.0995	0.9104
0.50	0.8260	0.6493	0.3049	3.7603	1.6588	2.9092	0.4994	-0.1745	0.6287	-0.0146	1.0230	-0.0820	0.9153
0.55	0.8250	0.6432	0.3023	3.7829	1.6884	2.9468	0.4627	-0.1960	0.6320	-0.0277	1.0270	-0.0688	0.9187
0.60	0.8239	0.6375	0.3003	3.7984	1.7133	2.9747	0.4354	-0.2113	0.6333	-0.0379	1.0268	-0.0588	0.9211
Coefficients for $a = 0.8$													
0.25	0.7736	0.6156	0.3003	3.5858	1.5991	2.6972	0.7201	-0.0148	0.5271	0.0401	0.8083	-0.1391	0.8777
0.30	0.7977	0.6235	0.3020	3.6648	1.6403	2.7901	0.5846	-0.0965	0.5674	0.0111	0.8909	-0.1061	0.8936
0.35	0.8107	0.6267	0.3021	3.7180	1.6738	2.8585	0.5108	-0.1457	0.5923	-0.0095	0.9413	-0.0845	0.9042
0.40	0.8172	0.6271	0.3013	3.7541	1.7015	2.9092	0.4653	-0.1776	0.6075	-0.0246	0.9712	-0.0694	0.9113
0.45	0.8201	0.6260	0.3001	3.7787	1.7245	2.9469	0.4347	-0.1993	0.6167	-0.0361	0.9883	-0.0584	0.9162
0.50	0.8212	0.6240	0.2990	3.7955	1.7438	2.9748	0.4126	-0.2144	0.6220	-0.0448	0.9974	-0.0502	0.9195
0.55	0.8215	0.6217	0.2979	3.8070	1.7599	2.9956	0.3962	-0.2253	0.6250	-0.0515	1.0016	-0.0438	0.9217
0.60	0.8214	0.6193	0.2970	3.8149	1.7733	3.0109	0.3835	-0.2331	0.6265	-0.0567	1.0029	-0.0389	0.9233
Coefficients for $a = 0.9$													
0.25	0.7959	0.6069	0.2917	3.7647	1.7496	2.9470	0.4195	-0.1917	0.5901	-0.0400	0.9328	-0.0532	0.9090
0.30	0.8086	0.6106	0.2942	3.7862	1.7650	2.9753	0.3976	-0.2116	0.6052	-0.0486	0.9609	-0.0453	0.9153
0.35	0.8148	0.6119	0.2952	3.8007	1.7777	2.9960	0.3834	-0.2244	0.6139	-0.0550	0.9766	-0.0396	0.9192
0.40	0.8179	0.6119	0.2954	3.8106	1.7883	3.0113	0.3730	-0.2331	0.6189	-0.0597	0.9851	-0.0353	0.9217
0.45	0.8193	0.6113	0.2953	3.8173	1.7971	3.0225	0.3651	-0.2392	0.6217	-0.0634	0.9895	-0.0320	0.9234
0.50	0.8199	0.6104	0.2951	3.8219	1.8045	3.0309	0.3589	-0.2436	0.6233	-0.0662	0.9915	-0.0294	0.9245
0.55	0.8201	0.6094	0.2949	3.8250	1.8106	3.0370	0.3539	-0.2467	0.6241	-0.0684	0.9921	-0.0273	0.9252
0.60	0.8202	0.6084	0.2947	3.8271	1.8157	3.0415	0.3499	-0.2490	0.6244	-0.0701	0.9919	-0.0257	0.9257

2.5 Secondary resonance and applicability of (15)–(19)

First, we have to remember that the Galerkin method of Part 1 provides stable calculations of the natural modes only for $a \geq 0.3$ and $h_1 \geq 0.1$. Physical and numerical treatments of this point were given in Part 1. Further, our numerical experiments in the Appendix show that the hydrodynamic coefficients d_i stably converge only for $a \geq 0.38$ and $h_1 \geq 0.2$. A physical explanation of this new limitation is associated with occurrence of a nonlinear shallow-water flow over the baffle for relatively small $h_1/(1-a)$.

Second, several combinations of h_1, h_2 and a may lead to secondary resonance, for which the five-mode solution (14) fails and some of $\beta_{2,i}^c, \beta_{2,i}^s, \beta_{0,i}^c, \beta_{0,i}^s, i \geq 1$ must be considered of the order $O(\epsilon^{1/3})$. The secondary resonance was discussed by Bryant [53] (circular basin); it was extensively examined for large-amplitude forcing by Faltinsen and Timokha [14, 54] (rectangular tank), Ockendon et al. [49], La Rocca et al. [32, 33] and Faltinsen et al. [24] (square base tank). Following Bryant [53], we expect secondary resonances as

$$R_{0i} = \frac{1}{2} \sqrt{\frac{\kappa_i^{(0)}}{\kappa_1^{(1)}}} \quad \text{or} \quad R_{2i} = \frac{1}{2} \sqrt{\frac{\kappa_i^{(2)}}{\kappa_1^{(1)}}}, \quad i \geq 1 \quad (21)$$

passes to 1. Our numerical analysis shows that only R_{22} and R_{02} can be equal to 1. Figure 3 illustrates this fact by curves r_{22} and r_{02} coupling the critical combinations of a and h_1 . In a small neighbourhood of these curves in the (a, h_1) -plane, $\beta_{0,2}^c$ and $\beta_{2,2}^c \sim \beta_{2,2}^s = O(\epsilon^{1/3})$ and, therefore, the system (15)–(19) is not applicable.

3 Steady-state resonant waves

The steady-state waves in a circular cylindrical tank without baffles are restricted to ‘planar’ and ‘swirling’ regimes. Their stability changes with the forcing frequency and amplitude [12, 13, 20, 21, 35, 44]. These regimes are best classified in terms of the two conjugate lowest-order modes. A spherical-pendulum analogy is also useful. Assuming a harmonic horizontal forcing, we observe that the ‘planar’ regime involves only one lowest-order mode. In view of the pendulum analogy, this regime corresponds to a planar motion

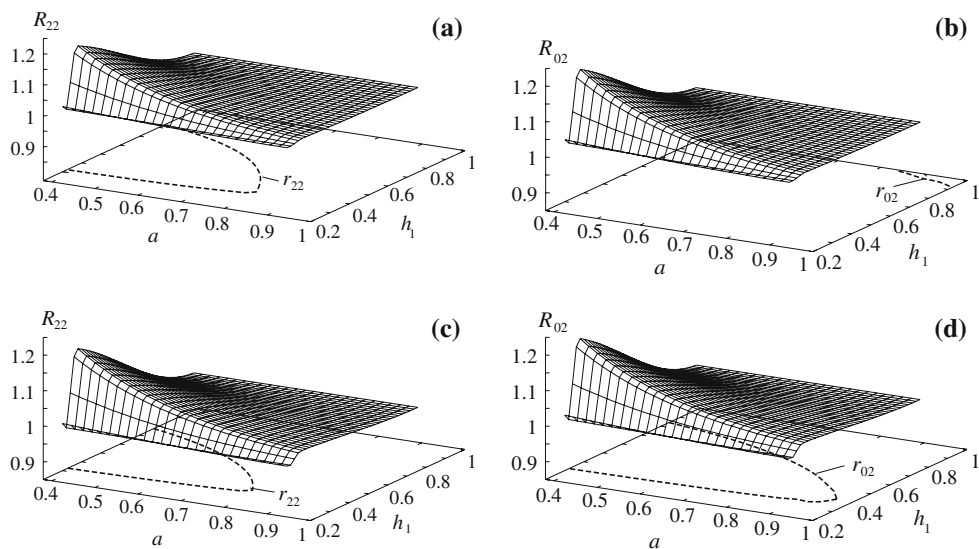


Fig. 3 Resonance detuning parameters R_{22} and R_{02} for $h_1 + h_2 = 1$ (first row) and for $h_1 + h_2 = 2$ (second row)

in the excitation plane. ‘Swirling’ or ‘rotary wave’ involves both dominating modes. It appears as an analogy of rotary motions of the spherical pendulum. Because the modal equations (15)–(19) are similar to those for a circular tank without baffles [21], the same two regimes for the baffled sloshing are expected.

3.1 Steady-state regimes

Considering the harmonic horizontal forcing (2) and accounting for (13), we obtain the dominating components for the lowest conjugate modes $\tilde{F}_1^{(1)}(r) \cos \theta$ and $\tilde{F}_1^{(1)}(r) \sin \theta$ as follows:

$$\begin{aligned} \beta_{1,1}^c(t) &= A \cos \sigma t + \bar{A} \sin \sigma t + o(\epsilon^{1/3}), \\ \beta_{1,1}^s(t) &= \bar{B} \cos \sigma t + B \sin \sigma t + o(\epsilon^{1/3}). \end{aligned} \tag{22}$$

Setting (22) in (17)–(19) and using the Fredholm alternative computes the second-order component, we have:

$$\begin{aligned} \beta_{0,1}^c(t) &= c_0 + c_1 \cos 2\sigma t + c_2 \sin 2\sigma t + o(\epsilon^{2/3}), \\ \beta_{2,1}^c(t) &= s_0 + s_1 \cos 2\sigma t + s_2 \sin 2\sigma t + o(\epsilon^{2/3}), \\ \beta_{2,1}^s(t) &= e_0 + e_1 \cos 2\sigma t + e_2 \sin 2\sigma t + o(\epsilon^{2/3}). \end{aligned} \tag{23}$$

Here

$$\begin{aligned} c_0 &= l_0(A^2 + \bar{A}^2 + B^2 + \bar{B}^2); \quad c_1 = p_0(A^2 - \bar{A}^2 - B^2 + \bar{B}^2), \\ c_2 &= 2p_0(A\bar{A} + B\bar{B}); \quad s_0 = l_2(A^2 + \bar{A}^2 - B^2 - \bar{B}^2), \\ s_1 &= p_2(A^2 - \bar{A}^2 + B^2 - \bar{B}^2); \quad s_2 = 2p_2(A\bar{A} - B\bar{B}), \\ e_0 &= -2l_2(A\bar{B} + B\bar{A}); \quad e_1 = 2p_2(\bar{A}B - A\bar{B}), \\ e_2 &= -2p_2(AB + \bar{A}\bar{B}) \end{aligned} \tag{24}$$

and

$$\begin{aligned} p_0 &= \frac{D_{10} + D_8}{2(\bar{\sigma}_0^2 - 4)}, \quad l_0 = \frac{D_{10} - D_8}{2\bar{\sigma}_0^2}, \\ p_2 &= \frac{D_9 + D_7}{2(\bar{\sigma}_2^2 - 4)}, \quad l_2 = \frac{D_9 - D_7}{2\bar{\sigma}_2^2}; \quad \bar{\sigma}_m = \frac{\omega_1^{(m)}}{\sigma}, \quad m = 0, 1, 2. \end{aligned} \tag{25}$$

By substituting (22) and (23) in (15)–(16) and using the Fredholm alternative, we get the following system of algebraic equations with respect to four variables A, \bar{A}, B and \bar{B}

$$\left. \begin{aligned} A[\bar{\sigma}_1^2 - 1 + m_1(A^2 + \bar{A}^2 + \bar{B}^2) + m_2B^2] + m_3\bar{A}B\bar{B} &= \Lambda\epsilon, \\ \bar{A}[\bar{\sigma}_1^2 - 1 + m_1(A^2 + \bar{A}^2 + B^2) + m_2\bar{B}^2] + m_3AB\bar{B} &= 0, \\ B[\bar{\sigma}_1^2 - 1 + m_1(B^2 + \bar{A}^2 + \bar{B}^2) + m_2A^2] + m_3\bar{B}A\bar{A} &= 0, \\ \bar{B}[\bar{\sigma}_1^2 - 1 + m_1(A^2 + B^2 + \bar{B}^2) + m_2\bar{A}^2] + m_3\bar{A}A\bar{B} &= 0, \end{aligned} \right\} \tag{26}$$

where the coefficients

$$\begin{aligned} m_1 &= D_5 \left(\frac{1}{2}p_0 - l_0 \right) - D_3 \left(\frac{1}{2}p_2 - l_2 \right) - 2D_6p_0 - 2D_4p_2 - \frac{1}{2}D_1, \\ m_2 &= -D_3 \left(l_2 + \frac{3}{2}p_2 \right) - D_5 \left(l_0 + \frac{1}{2}p_0 \right) + 2D_6p_0 - 6D_4p_2 + \frac{1}{2}D_1 - 2D_2, \\ m_3 &= m_1 - m_2 \end{aligned} \tag{27}$$

depend on σ, h_1, h_2 and a .

Further, accounting for the limit $\bar{\sigma}_1 \rightarrow 1$ and the asymptotics $A \sim \bar{A} \sim B \sim \bar{B} = O(\epsilon^{1/3})$ we deduce that $\bar{\sigma}_1^2 - 1 = O(\epsilon^{2/3}); \quad m_i(\sigma, h_1, h_2, a) = m_i^0(h_1, h_2, a) + o(\epsilon^{1/3}), \quad i = 1, 2, 3,$

where the first relationship implies the so-called Moiseyev asymptotic detuning and $m_i^0 = m_i(\omega_1^{(1)}, h_1, h_2, a) = O(1)$ (computing m_i^0 means $\sigma \equiv \omega_1^{(1)}$ in (25)).

When analysing similar algebraic systems, Gavriluk et al. [21] and Faltinsen et al. [54] showed that their resolvability condition reads

$$A \neq 0; \quad \bar{B} = \bar{A} = 0; \quad m_3^0 \neq 0. \tag{29}$$

By fixing the overall fluid depth $h = h_1 + h_2$, we may evaluate the coefficient m_3^0 versus h_1 and a . Zeros of m_3^0 , which imply that (26) cannot be solved, correspond to the curve γ_3 in the (a, h_1) -plane, as demonstrated in Fig. 4. Shapes and location of γ_3 are almost invariant for $h \geq 1$.

Considering fixed a and h_1 away from γ_3 and neglecting the $o(\epsilon)$ -terms, we may rewrite (26) in the following form

$$A(\bar{\sigma}_1^2 - 1 - m_1^0 A^2 - m_2^0 B^2) = \epsilon \Lambda; \quad B(\bar{\sigma}_1^2 - 1 - m_1^0 B^2 - m_2^0 A^2) = 0. \tag{30}$$

Solutions of (30) are functions of $\sigma/\omega_1^{(1)} = 1/\bar{\sigma}_1$. Accounting for the second equation of (30), which is always fulfilled as $B = 0$, yields two types of solutions. These are

(i) ‘planar’ waves

$$f(r, \theta, t) = A\tilde{F}_1^{(1)}(r) \cos \theta \cos \sigma t + o(\epsilon^{1/3}) \tag{31}$$

occurring for $B = 0$. The unique dominating amplitude A is then a root of the algebraic equation

$$A(\bar{\sigma}_1^2 - 1 + m_1^0 A^2) = \Lambda \epsilon. \tag{32}$$

(ii) ‘swirling’ waves

$$f(r, \theta, t) = \tilde{F}_1^{(1)}(r)(A \cos \theta \cos \sigma t \pm B \sin \theta \sin \sigma t) + o(\epsilon^{1/3}) \tag{33}$$

Fig. 4 m_3^0 versus (h_1, a) for $h_1 + h_2 = 1$

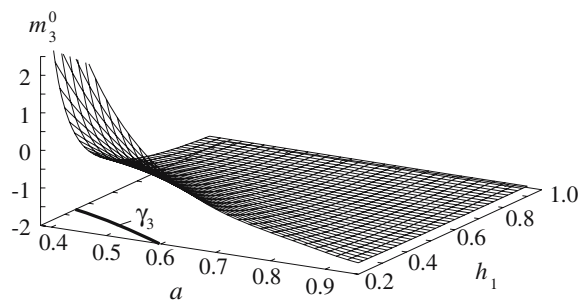
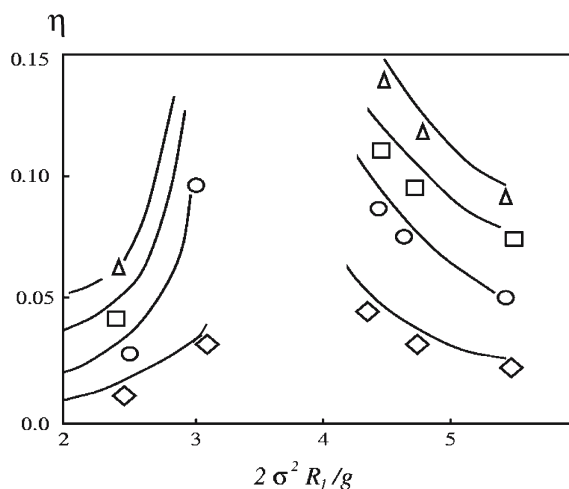


Fig. 5 Comparison with experiments by Hutton [55] and Abramson [35] for a circular cylindrical tank without baffles. ‘Planar’ steady-state regimes, the depth/radius ratio $h/R_1 = 2$. Calculated and measured values are presented for ϵ : $\Delta - \epsilon = 0.0454$; $\square - \epsilon = 0.0344$; $\circ - \epsilon = 0.023$; $\diamond - \epsilon = 0.0112$



occurring for $B \neq 0$. The first dominating amplitude A is then defined by

$$A(\bar{\sigma}_1^2 - 1 + m_4^0 A^2) = m_5 \Lambda \epsilon, \quad m_5^0 = -\frac{m_1^0}{m_3^0}, \quad m_4^0 = m_1^0 + m_2^0, \tag{34}$$

but the second lowest-order amplitude B is expressed via A as

$$B^2 = \frac{1}{m_1^0} (\bar{\sigma}_1^2 - 1 + m_2^0 A^2) > 0. \tag{35}$$

The \pm ahead of B in (33) implies either a clockwise or a counterclockwise rotary wave. Since both signs are mathematically possible, the initial conditions and transients should determine the sign.

Existence and stability of these two steady-state regimes are a function of the coefficients m_1 and m_2 and, in turn, a function of the geometric parameters h_1, h_2 and a . The regimes depend also on the forcing ϵ and $\bar{\sigma}_1 = \omega_1^{(1)}/\sigma$.

3.2 Stability

The stability of ‘planar’ and ‘swirling’ regimes can be studied by combining the first Lyapunov method and the multi-timing technique (see, [13] and [24]). This technique introduces the slowly varying time $\tau = \epsilon^{2/3} \sigma t / 2$ and expresses the infinitesimally perturbed dominating terms as

$$\begin{aligned} \beta_{1,1}^c &= (A + \alpha(\tau)) \cos \sigma t + \bar{\alpha}(\tau) \sin \sigma t + o(\epsilon^{1/3}), \\ \beta_{1,1}^s &= \bar{\beta}(\tau) \cos \sigma t + (B + \beta(\tau)) \sin \sigma t + o(\epsilon^{1/3}), \end{aligned} \tag{36}$$

where A and B are solutions of (30) and $\alpha, \bar{\alpha}, \beta$ and $\bar{\beta}$ are relative perturbations depending on τ .

Inserting (36) into (15)–(19), collecting terms of the lowest asymptotic order and keeping linear terms in $\alpha, \bar{\alpha}, \beta$ and $\bar{\beta}$ leads to the following linear system of ordinary differential equations

$$\mathbf{c}' + \mathcal{C}\mathbf{c} = 0. \tag{37}$$

Further, $\mathbf{c} = (\alpha, \bar{\alpha}, \beta, \bar{\beta})^T$ and the matrix \mathcal{C} has the following non-zero elements

$$\begin{aligned} c_{12} &= -[\bar{\sigma}_1^2 - 1 + m_1^0 A^2 + m_1^0 B^2]; & c_{21} &= \bar{\sigma}_1^2 - 1 + 3m_1^0 A^2 + m_2^0 B^2, \\ c_{14} &= -(m_1^0 - m_2^0)AB; & c_{41} &= -2m_2^0 AB, \\ c_{23} &= 2ABm_2^0; & c_{32} &= (m_1^0 - m_2^0)AB, \\ c_{34} &= \bar{\sigma}_1^2 - 1 + m_1^0 B^2 + m_1^0 A^2; & c_{43} &= -[\bar{\sigma}_1^2 - 1 + 3m_1^0 B^2 + m_2^0 A^2]. \end{aligned}$$

The fundamental solution of the Hamiltonian system (37) depends on the eigenvalue problem $\det[\lambda E + \mathcal{C}] = 0$, where E is the identity matrix. Computations lead to the following characteristic polynomial

$$\lambda^4 + c_1 \lambda^2 + c_0 = 0, \tag{38}$$

where c_0 is the determinant of \mathcal{C} and c_1 is a complicated function of the elements of \mathcal{C} . The necessary and sufficient condition for the real part of the quartic equation (38) to be non-positive, i.e., for the steady-state solutions be stable, is ([13])

$$c_0 > 0; \quad c_1 > 0; \quad c_1^2 - 4c_0 > 0. \tag{39}$$

Here c_0 vanishes at the turning-point solutions and at the Poincaré bifurcation points. The zeros of the discriminant $c_1^2 - 4c_0$ are Hamiltonian Hopf-bifurcation points where the real parts of a pair of complex-conjugate zeros of c_0 becomes positive.

3.3 Validation by experiments

To the authors' knowledge, the literature does not contain experimental data about steady-state resonant regimes in baffled circular cylindrical tanks. These exist only for the non-baffled case (see [55], [35] and, recently, [56]). Measurements of the wave elevation as well as detection of the effective frequency domain have mostly been reported for the 'planar' regime. Complications in measuring the amplitude responses for 'swirling' are caused by the occurrence of breaking waves. See, for details [56] and, for 'swirling' in a square-base tank, [57].

Assuming $a = 1$ and using results of Sects. 3.1 and 3.2, we compared our theoretical prediction with [35]. The original experimental data were normalised as the half-sum of two diametrically opposite wave elevations near the wall in the plane of excitations to the radius R_1 . In our modal representation, this implies

$$\eta = \frac{1}{2} \max_{t \in [0, 2\pi/\sigma]} (|\beta_{0,1}^c + \beta_{1,1}^c - \beta_{2,1}^c| + |\beta_{0,1}^c - \beta_{1,1}^c - \beta_{2,1}^c|) \quad (40)$$

provided by the non-dimensional steady-state solution (22) + (23).

Comparison for different non-dimensional forcing amplitudes is presented in Fig. 5. It demonstrates good agreement.

3.4 Response curves

The appearance and stability of 'planar' and 'swirling' flows depend on the signs and the absolute values of m_1^0 and m_4^0 . For a fairly large fluid depth ($h = h_1 + h_2 \geq 1$), our numerical analysis found that $m_4^0 > 0$, but m_1^0 can change sign on a curve γ_1 belonging to the (a, h_1) -plane. This is illustrated in Fig. 6(a, b), where M_1^+ and M_1^- are the areas of positive and negative m_1^0 , respectively. Evaluating the response curves in the $(1/\bar{\sigma}_1, |A|)$ -plane, we conclude that 'swirling' is always characterised by 'hard-spring' behaviour, but 'planar' may change from 'soft' (in M_1^-) to 'hard-spring' (in M_1^+) behaviour.

The lowest-order amplitudes A and B characterise two perpendicular wave profiles. A implies a wave component in the plane of excitation (in-phase with forcing), but B is perpendicular to the plane of excitation (out-of-phase by 90°). This means that the response curves are best illustrated in the $(1/\bar{\sigma}_1, |A|, |B|)$ -space. Figure 7(a–f) demonstrate the response curves for $h_1 = 0.3$, $h_1 + h_2 = 1$ and $\epsilon = 0.002$. The columns (sub-figures) a–f are ordered for decreasing a , where sub-figure (a) implies a tank without baffles. A three-dimensional view is accompanied by projections on both the $(1/\bar{\sigma}_1, |A|)$ and $(1/\bar{\sigma}_1, |B|)$ -planes. The solid line is used for stable solutions, but the dashed line denotes unstable ones.

Figure 7(a) starts with $a = 1$ (tank without baffle). This type of branching was analysed by Miles [12, 13], Lukovsky [20], Lukovsky and Timokha [29] and Gavriluk et al. [21]. The analysis exhibits a turning point

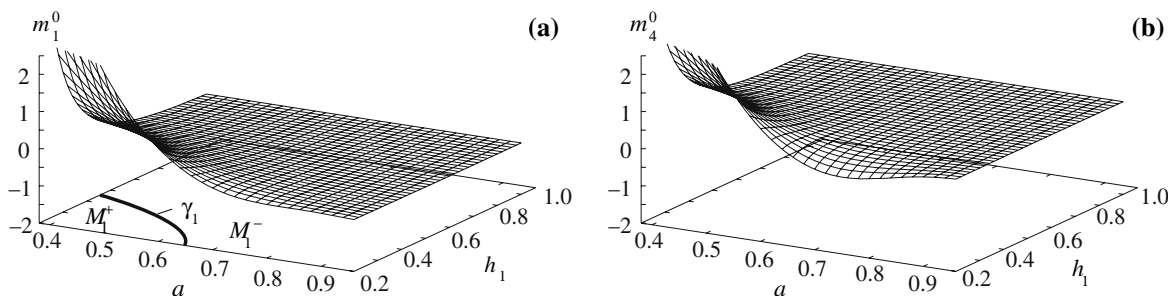


Fig. 6 $m_1^{(0)}$ and $m_4^{(0)}$ vs. a and h_1 for $h_1 + h_2 = 1$

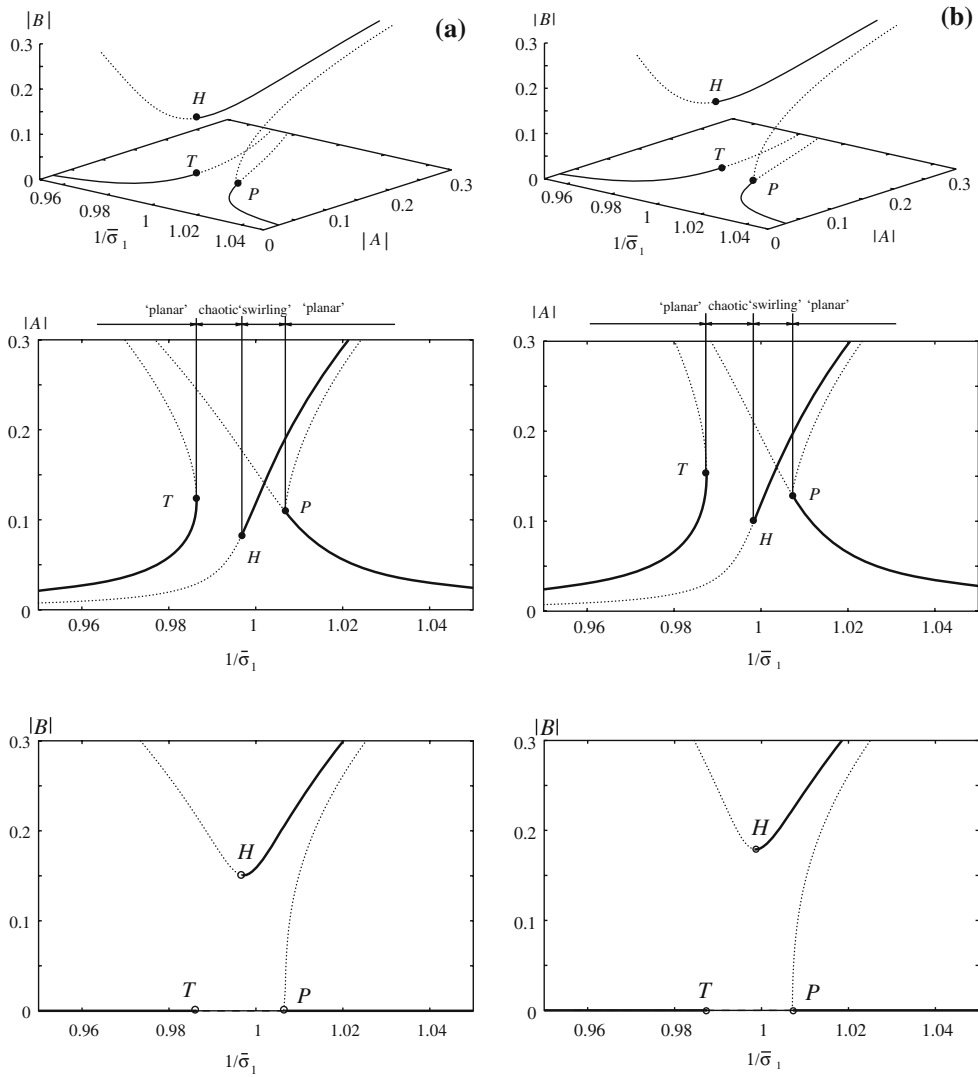


Fig. 7 Response curves for $\epsilon = 0.002, h_1 + h_2 = 1$ and $h_1 = 0.3$. Each column gives the response curves in the $(1/\bar{\sigma}_1, |A|, |B|)$ -space and their projections on the $(1/\bar{\sigma}_1, |A|)$ - and $(1/\bar{\sigma}_1, |B|)$ -planes. The solid line corresponds to stable, but the dashed line—to unstable steady-state solutions. The effective frequency domains for ‘planar’ and ‘swirling’ regimes are presented in the $(1/\bar{\sigma}_1, |A|)$ -plane. The ‘chaotic’ domain is caused by instability of both steady-state regimes. **(a)**—The tank has no baffle ($a = 1$), T is the turning point of the ‘planar’ response curve, P is the Poincare-bifurcation point, where unstable ‘swirling’ emerges from ‘planar’ solutions and H is the Hamiltonian Hopf-bifurcation point. **(b)**—The same as **(a)**, but for $a = 0.7$. **(c)**—The same as **(a)**, but for $a = 0.6$. **(d)**—The same as **(a)**, but for $a = 0.5$. Here, T is the turning point for the ‘planar’ response curve, P_1 implies the Poincare-bifurcation point, T_1 is the turning point for ‘swirling’ and $H_i, i = 1, 2$ are the Hamiltonian Hopf-bifurcation points. **(e)**—The same as **(d)**, but for $a = 0.44$. Here, P_2 is the Poincare-bifurcation point, H is the Hamiltonian Hopf-bifurcation point, T is the turning point for ‘planar’. **(f)**—The same as **(e)**, but for $a = 0.4$

T for the ‘planar’ response curve, a Poincare-bifurcation point P , from which ‘planar’ response curve may bifurcate to ‘swirling’ (this fact is demonstrated by a three-dimensional view), and a Hamiltonian Hopf-bifurcation point H , where the ‘swirling’ changes its stability feature. The effective frequency domains of stable ‘planar’ and ‘swirling’ are marked in the $(1/\bar{\sigma}_1, |A|)$ -plane. These domains imply intervals on the $1/\bar{\sigma}_1$ -axis, on which the denoted wave regime exist, are stable and have minimum kinetic energy with respect to other stable steady-state waves. In addition, we introduced a ‘chaotic’ frequency domain. In this

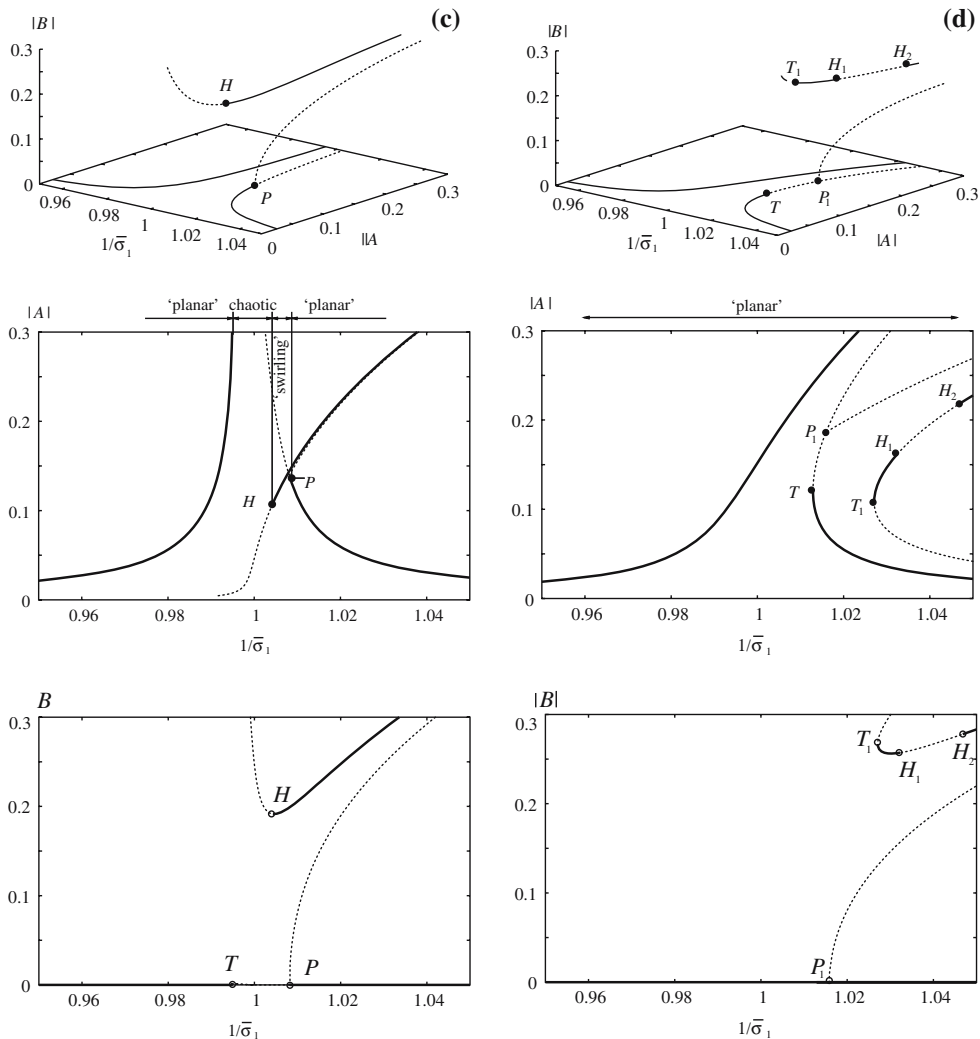


Fig. 7 continued

range, our analysis has not been able to establish any stable steady-state waves and irregular waves were detected in [35, 55, 56]. As shown in Fig. 7(b), a small-size annular baffle does not change this branching. There is a small drift of the ‘chaotic’ domain, but its range (interval between abscissas of T and H) is mostly the same as in Fig. 7(a).

“Migration” of the ‘chaotic’ frequency domain becomes visible only if $(a, h_1) \in M_1^-$ is close to γ_1 in Fig. 6(a). The situation is depicted in Fig. 7(c) drawn for $a = 0.6$. The Hamiltonian Hopf-bifurcation point H moves then to the right and projections of the two ‘swirling’ response curves on the $(1/\bar{\sigma}_1, |A|)$ -plane are situated close to each other.

When (a, h_1) runs into M_1^+ in Fig. 6(a), the branching changes dramatically. Examples are given in Fig. 7(d–f) for $a = 0.5, 0.44$ and 0.4 , respectively. The ‘planar’ response curves are then characterised by a ‘hard-spring’ behaviour. As a result, the turning point T is situated on the right sub-branch. Besides, the frequency domain of ‘chaotic’ motions disappears and the response curves responsible for ‘swirling’ move away from the primary resonance $1/\bar{\sigma}_1 = 1$. In the case $a = 0.5$ depicted in Fig. 7(d), the ‘planar’ regime is stable for either $1/\bar{\sigma}_1$ close to 1 and ‘swirling’ is not realised. Stable ‘swirling’ between the turning point T_1 and the Hamiltonian Hopf-bifurcation point H_1 and in a zone to the right of H_2 is characterised by a

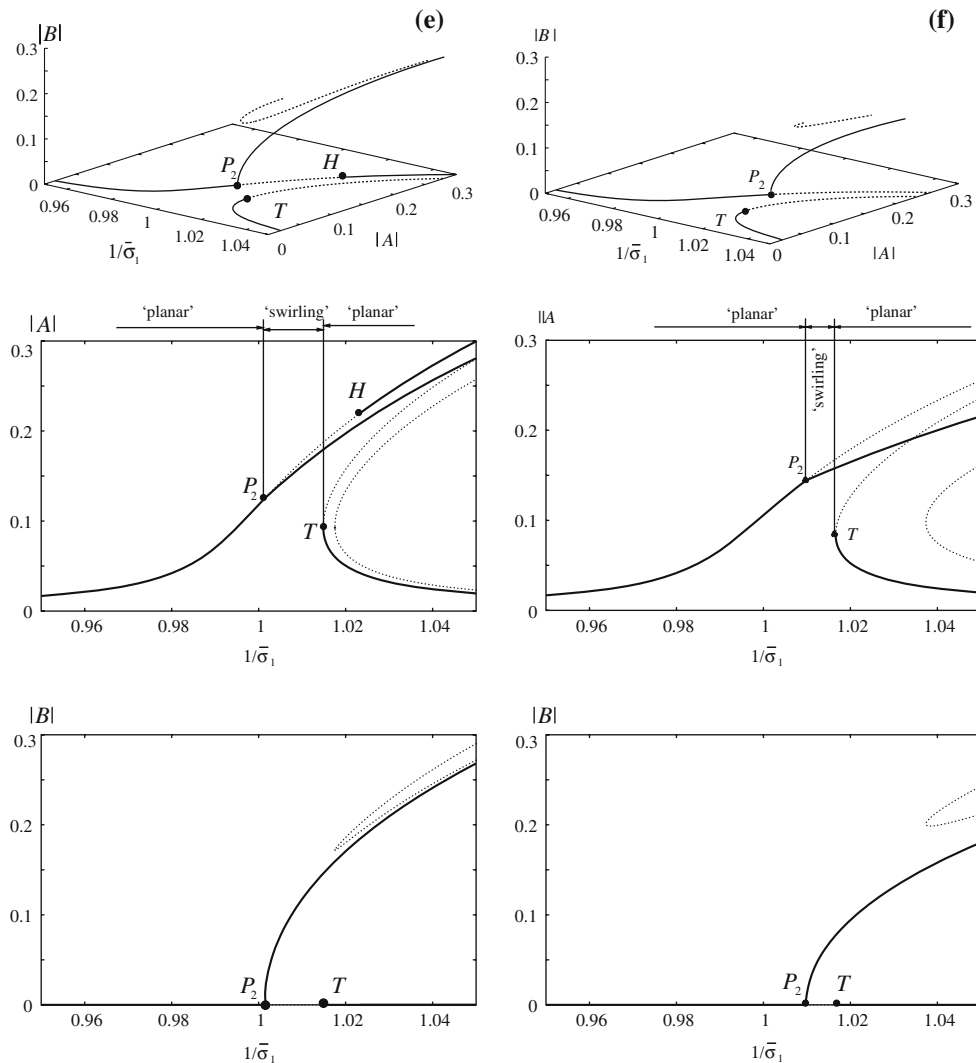


Fig. 7 continued

higher kinetic energy than in the ‘planar’ case. Figure 7(e,f) shows that T_1 , H_1 and H_2 -bifurcation points disappear with decreasing a down to 0.4. Here, the Poincare-bifurcation point P_1 “jumps” to P_2 , i.e., from the right to the left ‘planar’ sub-branch. In addition, there is a frequency domain where our theory expects stable ‘swirling’, but unstable ‘planar’ waves.

Evolution of the branching in Fig. 7(a–f) versus a is typical for $h_1 + h_2 \geq 1$ and $h_1 \leq 0.45$. When $h_1 > 0.45$ the branching always is similar to that in Fig. 7(a, b). This means that, if the annular baffle is immersed deep into fluid, the weakly nonlinear resonant sloshing is qualitatively the same as in a circular cylindrical tank without baffles.

Summarising, the branchings versus a and h_1 with $h_1 + h_2 \geq 1$ lead us to conclude that the response curves behave as in Fig. 7(a–c) for $(a, h_1) \in M_1^-$ (see, Fig. 6(a)). The response curves illustrated in Fig. 7(e, f) may be found only for $(a, h_1) \in M_1^+$. In particular, evaluating the branching versus h_1 for a fixed $a > 0.65$, we observe curves similar to those established in Fig. 7(a, b). Physically, this means that a small-sized annular baffle does not affect the nonlinear resonant steady-state waves. It should, however, yield vortex-induced damping, whose influence will be addressed in Part 3.

Finally, varying the non-dimensional forcing amplitude ϵ for $h_1 + h_2 \geq 1$ and $h_1 \leq 0.45$ does not change the types of the branching illustrated in Fig. 7(a–f). However, the frequency domain of ‘chaotic’ motions increases with increasing ϵ . This result may also be corrected by accounting for damping.

4 Conclusions

In the present paper a weakly nonlinear modal theory of sloshing in a baffled circular cylindrical tank has been proposed. The asymptotic modal method by Narimanov [43] has been used. A system of nonlinear ordinary differential equations (modal system) coupling the five lowest natural modes was derived. The system is a direct generalisation of an analogous five-dimensional system by Dodge et al. [50], Lukovsky [20], Gavriluyk et al. [21] and Ikeda and Murakami [27] that was developed for a circular cylindrical tank without baffles. In the absence of secondary resonance, the usage of the five-mode solution for the non-baffled tank was justified by Miles [12, 13] and Lukovsky [20]. This explains why the five-mode solution is applicable to the case studied here. Occurrence of the secondary resonance versus the size and the position of the baffle was estimated to confirm that this resonance and consequent amplification of higher second-order modes may be important only for a few isolated geometric configurations.

The asymptotic modal system is applicable for the scaled (by radius) width of the ring baffle $(1-a) \leq 0.62$ and the scaled height of the fluid layer over the baffle $h_1 \geq 0.2$. These limitations are in part associated with numerical problems discussed in Part 1 as well as with convergence to the coefficients of the modal system. Physically, small $h_1/(1-a)$ implies also a shallow-water flow over the horizontal baffle. This flow is strongly dissipative and cannot be described by our inviscid-fluid model. Besides the effect of the vortices shed from the baffle edge near the free surface, as well as a penetration of the free surface by the baffle for large-amplitude sloshing, may play a role. This means that the case of small h_1 (especially with a small overall depth $h = h_1 + h_2$) needs a dedicated study based on the Navier–Stokes formulation.

The modal system was used to study steady-state resonant fluid motions due to lateral excitations of the lowest natural frequency. The analysis concentrated on the case of the overall fluid depth to the radius ratio $h = h_1 + h_2 \geq 1$. It established two and only two steady-state regime, i.e., ‘planar’ and ‘swirling’. In the particular case of a non-baffled tank, results have been validated by experimental data from [35]. The behaviour of the response curves has been studied versus a and h_1 .

Our studies do not account for damping. Its accurate quantification should lead to new terms in our nonlinear modal system. These are responsible for shear ([58]) and vorticity stresses ([10, 11, 59]). Forthcoming Part 3 will focus on the modified system. It is of primary interest for small-sized baffles. As one can see from our analysis, a small annular baffle does not influence the effective frequency domains of both ‘planar’ and ‘swirling’ regimes. However, damping may affect them. This was shown by Miles [13] who tested speculatively large damping rates for a circular cylindrical tank without baffles. He has shown in particular that the range of ‘chaotic’ waves may decrease considerably and even disappear. On the other hand, decreasing the hole in an annular baffle decreases a flux between the upper and lower fluid sub-domains. This is because the two lowest-order modes are characterised by a zero vertical velocity component in the centre. In that case, the vortex shedding is basically formed by the second-order terms, which are small. As a result, we do not expect a substantial effect of vortex-induced damping when a decreases.

Appendix

In order to derive expressions for d_i , $i = 1, \dots, 8$, we had to find first- and second-order solutions of (11) in terms of $\tilde{\beta}_{mi}(t)$. This is a straightforward, but tedious analytical task. By denoting

$$\mathcal{G}_1 = \frac{\partial \tilde{F}_1^{(1)}}{\partial r} \frac{\partial \psi_1^{(1,1)}}{\partial r} - \tilde{F}_1^{(1)} \frac{\partial^2 \psi_1^{(1,1)}}{\partial z^2}; \quad \mathcal{G}_2 = \frac{1}{r^2} \tilde{F}_1^{(1)} \psi_1^{(1,1)},$$

$$\mathcal{G}_3 = \frac{1}{2} \left[\frac{\partial}{\partial r} \left((\tilde{F}_1^{(1)})^2 \frac{\partial^2 \psi_1^{(1,1)}}{\partial z \partial r} \right) + \frac{(\tilde{F}_1^{(1)})^2}{r} \frac{\partial^2 \psi_1^{(1,1)}}{\partial z \partial r} - \frac{\partial \psi_1^{(1,1)}}{\partial z} \frac{(\tilde{F}_1^{(1)})^2}{r^2} \right],$$

$$\mathcal{G}_5 = \frac{\partial}{\partial r} \left(\tilde{F}_1^{(1)} \frac{\partial \Psi_0}{\partial r} + \frac{\tilde{F}_1^{(1)}}{r} \frac{\partial \Psi_0}{\partial r} \right); \quad \mathcal{G}_7 = \frac{2\tilde{F}_1^{(1)}}{r^2} \Psi_2,$$

$$\mathcal{G}_6 = \frac{\partial}{\partial r} \left(\tilde{F}_1^{(1)} \frac{\partial \Psi_2}{\partial r} \right) + \frac{\tilde{F}_1^{(1)}}{r} \frac{\partial \Psi_2}{\partial r} - 4 \frac{\tilde{F}_1^{(1)}}{r^2} \Psi_2,$$

$$\mathcal{G}_{01} = \frac{\partial \tilde{F}_1^{(0)}}{\partial r} \frac{\partial \psi_1^{(1,1)}}{\partial r} - \tilde{F}_1^{(0)} \frac{\partial^2 \psi_1^{(1,1)}}{\partial z^2},$$

$$\mathcal{G}_{12} = \frac{\partial \tilde{F}_1^{(1)}}{\partial r} \frac{\partial \psi_1^{(2,1)}}{\partial r} - \tilde{F}_1^{(1)} \left(\frac{\partial^2 \psi_1^{(2,1)}}{\partial z^2} - \frac{2}{r^2} \psi_1^{(2,1)} \right),$$

$$\mathcal{G}_{21} = \frac{\partial \tilde{F}_1^{(2)}}{\partial r} \frac{\partial \psi_1^{(1,1)}}{\partial r} + \tilde{F}_1^{(2)} \left(\frac{1}{r^2} \psi_1^{(1,1)} - \frac{\partial^2 \psi_1^{(1,1)}}{\partial z^2} \right),$$

where $\Psi_0(z, r)$ and $\Psi_2(z, r)$ are solutions of the following Neumann boundary-value problems in the meridional plane G :

$$\left. \begin{aligned} L_0(\Psi_0) = 0 \quad \text{in } G; \quad |\Psi_0(z, 0)| < \infty, \\ \frac{\partial \Psi_0}{\partial \nu} = 0 \quad \text{on } L_1; \quad \frac{\partial \Psi_0}{\partial \nu} = \frac{1}{2}(\mathcal{G}_1 + \mathcal{G}_2) \quad \text{on } L_0, \end{aligned} \right\} \tag{41}$$

$$\left. \begin{aligned} L_2(\Psi_2) = 0 \quad \text{in } G; \quad |\Psi_2(z, 0)| < \infty, \\ \frac{\partial \Psi_2}{\partial \nu} = 0 \quad \text{on } L_1; \quad \frac{\partial \Psi_2}{\partial \nu} = \frac{1}{2}(\mathcal{G}_1 - \mathcal{G}_2) \quad \text{on } L_0 \end{aligned} \right\} \tag{42}$$

(see, geometrical definitions in Fig. 2), we get

$$d_1 = \frac{\pi}{4} \int_{L_0} \left[(3\mathcal{G}_1 + 2\mathcal{G}_2)(\tilde{F}_1^{(1)})^2 + (3\mathcal{G}_2 + 4\mathcal{G}_5 + 2\mathcal{G}_6 + 2\mathcal{G}_7)\psi_1^{(1,1)} + \frac{3}{2} \frac{\partial^2 \psi_1^{(1,1)}}{\partial z^2} \right] r dr,$$

$$d_2 = \frac{\pi}{4} \int_{L_0} \left[(\mathcal{G}_1 + 4\mathcal{G}_2)(\tilde{F}_1^{(1)})^2 + (\mathcal{G}_3 + 2\mathcal{G}_5)\psi_1^{(1,1)} + \frac{1}{2} \frac{\partial^2 \psi_1^{(1,1)}}{\partial z^2} (\tilde{F}_1^{(1)})^3 \right] r dr,$$

$$d_3 = \frac{\pi}{2} \int_{L_0} (\mathcal{G}_{21} \psi_1^{(1,1)} + (\tilde{F}_1^{(1)}) \tilde{F}_1^{(2)}) r dr,$$

$$d_4 = -\frac{\pi}{4} \int_{L_0} [\mathcal{G}_{12} \psi_1^{(1,1)} + (\mathcal{G}_1 - \mathcal{G}_2)\psi_1^{(2,1)} + 2(\tilde{F}_1^{(1)})^2 \tilde{F}_1^{(2)}] r dr,$$

$$d_5 = \pi \int_{L_0} (\psi_1^{(1,1)} \mathcal{G}_{01} + (\tilde{F}_1^{(1)})^2 \tilde{F}_1^{(0)}) r dr,$$

$$d_6 = \frac{\pi}{2} \int_{L_0} [\mathcal{G}_{01} \psi_1^{(1,1)} + (\mathcal{G}_1 + \mathcal{G}_2)\psi_1^{(0,1)} + 2(\tilde{F}_1^{(1)})^2 \tilde{F}_1^{(0)}] r dr,$$

$$d_7 = d_4 + \frac{1}{2}d_3; \quad d_8 = d_6 - \frac{1}{2}d_5; \quad \lambda = \pi \kappa_1^{(1)} \int_{L_0} r^2 \psi_1^{(1,1)} dr,$$

Table 2 Convergence to d_1 and d_2 versus I_0 in the Fourier series (43) ($a = 0.7$; $h_2 = 0.5$)

I_0	$h_1 = 0.3$		$h_1 = 0.5$	
	d_1	d_2	d_1	$-d_2$
1	0.91465	0.064550	0.52435	0.16810
2	1.00504	0.095611	0.53062	0.16729
3	1.01616	0.099171	0.53091	0.16729
4	1.01640	0.099204	0.53093	0.16728
5	1.01645	0.099239	0.53094	0.16728
6	1.01647	0.099245	0.53094	0.16728

$$\mu_{11} = \pi \int_{L_0} \tilde{F}_1^{(1)} \psi_1^{(1,1)} r dr; \quad \mu_{01} = 2\pi \int_{L_0} \tilde{F}_1^{(0)} \psi_1^{(0,1)} r dr, \quad \mu_{21} = \pi \int_{L_0} \tilde{F}_1^{(2)} \psi_1^{(2,1)} r dr.$$

Approximate solutions of (41) and (42) should be found with utilising the Fourier series by $\psi_i^{(0)}$ and $\psi_i^{(2)}$, $i \geq 1$ as follows

$$\Psi_0 = \lim_{I_0 \rightarrow \infty} \sum_{i=1}^{I_0} a_i \psi_i^{(0)}(z, r), \quad \Psi_2 = \lim_{I_0 \rightarrow \infty} \sum_{i=1}^{I_0} b_i \psi_i^{(2)}(z, r), \quad (43)$$

where

$$a_i = \frac{\int_{L_0} (\mathcal{G}_1 + \mathcal{G}_2) \psi_i^{(0)} r dr}{2\kappa_i^{(0)} \int_{L_0} r (\psi_i^{(0)})^2 dr}; \quad b_i = \frac{\int_{L_0} (\mathcal{G}_1 - \mathcal{G}_2) \psi_i^{(2)} r dr}{2\kappa_i^{(2)} \int_{L_0} r (\psi_i^{(2)})^2 dr}.$$

Equation (43) needs accurate approximations of the higher natural modes. These are given in Part 1. Convergence to d_1 and d_2 , which depend on $\Psi_0(z, r)$ and $\Psi_2(z, r)$, is illustrated in Table 2. It is fast for $h_1 \geq 0.2$ and $a \geq 0.38$. However, smaller h_1 and a give rise to slow convergence.

References

- Gavrilyuk I, Lukovsky IA, Trotsenko Yu, Timokha AN (2006) The fluid sloshing in a vertical circular cylindrical tank with an annular baffle. Part 1. Linear fundamental solutions. J Eng Math 54:71–88
- Colicchio G (2004) Violent disturbance and fragmentation of free surface. Ph.D. Thesis, School of Civil Engineering and the Environment, University of Southampton, UK
- Cariou A, Casella G (1999) Liquid sloshing in ship tanks: a comparative study of numerical simulation. Marine Struct 12:183–198
- Celebi SM, Akyildiz H (2002) Nonlinear modelling of liquid sloshing in a moving rectangular tank. Ocean Engng 29:1527–1553
- Colagrossi A, Landrini M (2003) Numerical simulation of interfacial flows by smoothed particle hydrodynamics. J Comp Phys 191:448–475
- Cole HA Jr. (1970) Effects of vortex shedding on fuel slosh damping prediction. NASA Technical Note, NASA TN D-5705, Washington DC, March, 28 pp
- Bogoryad IB, Druzhinina GZ (1985) On the damping of sloshing a viscous fluid in cylindrical tank with annular baffle. Soviet Appl Mech 21:126–128
- Mikishev GI (1978) Experimental methods in the dynamics of spacecraft. Moscow: Mashinostroenie, 247 pp (in Russian)
- Mikishev GI, Churilov GA (1977) Some results on the experimental determining of the hydrodynamic coefficients for cylinder with ribs. In: Bogoryad IB (ed.), Dynamics of elastic and rigid bodies interacting with a liquid. Tomsk: Tomsk university, pp. 31–37 (in Russian)
- Buzhinskii VA (1998) Vortex damping of sloshing in tanks with baffles. J Appl Math Mech 62:217–224
- Isaacson M, Premasiri S (2001) Hydrodynamic damping due to baffles in a rectangular tank. Canad. J Civil Engng 28:608–616
- Miles JW (1984) Internally resonant surface waves in circular cylinder. J Fluid Mech 149:1–14

13. Miles JW (1984) Resonantly forces surface waves in circular cylinder. *J Fluid Mech* 149:15–31
14. Faltinsen OM, Timokha AN (2001) Adaptive multimodal approach to nonlinear sloshing in a rectangular tank. *J Fluid Mech* 432:167–200
15. Cho JR, Lee HW (2003) Dynamic analysis of baffled liquid-storage tanks by the structural-acoustic finite element formulation. *J Sound Vibr* 258:847–866
16. Cho JR, Lee HW (2004) Numerical study on liquid sloshing in baffled tank by nonlinear finite element method. *Comp Methods Appl Mech Engng* 193:2581–2598
17. Cho JR, Lee HW (2004) Non-linear finite element analysis of large amplitude sloshing flow in two-dimensional tank. *Int J Num Methods Engng* 61:514–531
18. Cho JR, Lee HW, Ha SY (2005) Finite element analysis of resonant sloshing response in 2-D baffled tank. *J Sound Vibr* 288:829–845
19. Biswal KC, Bhattacharyya SK, Sinha PK (in press) Non-linear sloshing in partially liquid filled containers with baffles. *Int J Num Methods Engng* (in press)
20. Lukovsky IA (1990) Introduction to the nonlinear dynamics of a limited liquid volume. Kiev, Naukova Dumka, pp 220 (in Russian)
21. Gavriluk I, Lukovsky IA, Timokha AN (2000) A multimodal approach to nonlinear sloshing in a circular cylindrical tank. *Hybr Methods Engng* 2(4):463–483
22. Gavriluk I, Lukovsky I, Makarov V, Timokha A (2006) Evolutional problems of the contained fluid. Kiev, Publishing House of the Institute of Mathematics of NASU, 233 pp
23. Faltinsen OM, Rognebakke OF, Lukovsky IA, Timokha AN (2000) Multidimensional modal analysis of nonlinear sloshing in a rectangular tank with finite water depth. *J Fluid Mech* 407:201–234
24. Faltinsen OM, Rognebakke OF, Timokha AN (2003) Resonant three-dimensional nonlinear sloshing in a square base basin. *J Fluid Mech* 487:1–42
25. Faltinsen OM, Rognebakke OF, Timokha AN (2005) Classification of three-dimensional nonlinear sloshing in a square-base tank with finite depth. *J Fluids Struct* 20:81–103
26. Hill DH (2003) Transient and steady-state amplitudes of forced waves in rectangular tanks. *Phys Fluids* 15:1576–1587
27. Ikeda T, Murakami S (2005) Autoparametric resonances in a structure-fluid interaction system carrying a cylindrical liquid tank. *J Sound Vibr* 285:517–546
28. Ikeda T, Murakami S (2005) Nonlinear random responses of a structure parametrically coupled with liquid sloshing in a cylindrical tank. *J Sound Vibr* 284:75–102
29. Lukovsky IA, Timokha AN (1995) Variational methods in nonlinear dynamics of a limited liquid volume. Kiev, Institute of Mathematics, 400 pp (in Russian)
30. Rognebakke OF, Faltinsen OM (2003) Coupling of sloshing and ship motions. *J Ship Res* 47:208–221
31. Faltinsen OM, Rognebakke OF, Timokha AN (2005) Resonant three-dimensional nonlinear sloshing in a square base basin. Part 2. Effect of higher mode. *J Fluid Mech* 523:199–218
32. La Rocca M, Mele P, Armenio V (1997) Variational approach to the problem of sloshing in a moving container. *J Theoret Appl Fluid Mech* 1:280–310
33. La Rocca M, Sciortino G, Boniforti MA (2000) A fully nonlinear model for sloshing in a rotating container. *Fluid Dyn Res* 27:23–52
34. Faltinsen OM, Timokha AN (2002) Analytically-oriented approaches to two-dimensional fluid sloshing in a rectangular tank (survey). *Proc. Inst. Math. Ukrainian Nat Acad Sci* 44:321–345
35. Abramson HN (1966) The dynamics of liquids in moving containers. NASA Report, SP-106, 467 pp
36. Bredmose H, Brocchini M, Peregrine DH, Thais L (2003) Experimental investigation and numerical modelling of steep forced water waves. *J Fluid Mech* 490:217–249
37. Hermann M, Timokha A (2005) Modal modelling of the nonlinear resonant sloshing in a rectangular tank I: A single-dominant model. *Math. Models Methods Appl Sci* 15:1431–1458
38. Moore RE, Perko LM (1969) Inviscid fluid flow in an accelerating cylindrical container. *J Fluid Mech* 22:305–320
39. Perko LM (1969) Large-amplitude motions of liquid-vapour interface in an accelerating container. *J Fluid Mech* 35:77–96
40. Miles JW (1976) Nonlinear surface waves in closed basins. *J Fluid Mech* 75:419–448
41. Lukovsky IA (1976) Variational method in the nonlinear problems of the dynamics of a limited liquid volume with free surface. In book: *Oscillations of Elastic Constructions with Liquid*. Volna, Moscow, pp 260–264 (in Russian)
42. Hill D, Frandsen J (2005) Transient evolution of weakly nonlinear sloshing waves: an analytical and numerical comparison. *J Engng Math* 53:187–198
43. Narimanov GS (1957) Movement of a tank partly filled by a fluid: the taking into account of non-smallness of amplitude. *J Appl Math Mech (PMM)* 21:513–524 (in Russian)
44. Narimanov GS, Dokuchaev LV, Lukovsky IA (1977) Nonlinear Dynamics of flying Apparatus with Liquid. *Mashinostroenie, Moscow*, 203 pp (in Russian)
45. Gavriluk I, Lukovsky I, Timokha A (2005) Linear and nonlinear sloshing in a circular conical tank. *Fluid Dyn Res* 37:399–429
46. Moiseyev NN (1958) To the theory of nonlinear oscillations of a limited liquid volume. *J. Appl Math Mech* 22:860–872
47. Bogoljubov NN, Mitropolskii Yu (1961) *Asymptotic Methods in the Theory of Nonlinear Oscillations*. Gordon and Breach, New York

48. Ockendon JR, Ockendon H (1973) Resonant surface waves. *J Fluid Mech* 59:397–413
49. Ockendon H, Ockendon JR, Waterhouse DD (1996) Multi-mode resonance in fluids. *J Fluid Mech* 315:317–344
50. Dodge FT, Kana DD, Abramson HN (1965) Liquid surface oscillations in longitudinally excited rigid cylindrical containers. *AIAA J* 3:685–695
51. Moiseyev NN, Rumyantsev VV (1968) *Dynamic Stability of Bodies Containing Fluid*. Springer, New York, 326 pp
52. Lukovsky IA (2004) Variational methods of solving dynamic problems for fluid-containing bodies. *Int Appl Mech* 40:1092–1128
53. Bryant PJ (1989) Nonlinear progressive waves in a circular basin. *J Fluid Mech* 205:453–467
54. Faltinsen OM, Timokha AN (2002) Asymptotic modal approximation of nonlinear resonant sloshing in a rectangular tank with small fluid depth. *J Fluid Mech* 470:319–357
55. Hutton RE (1963) An investigation of nonlinear, non-planar oscillations of liquid in cylindrical containers, Technical Notes, NASA, D-1870, Washington, 145–153
56. Royon-Lebeaud A, Cartellier A, Hopfinger EJ Liquid sloshing and wave breaking in cylindrical and square-base containers. *J Fluid Mech* (under consideration)
57. Faltinsen OM, Rognebakke OF, Timokha AN (2006) Transient and steady-state amplitudes of resonant three-dimensional sloshing in a square base tank with a finite fluid depth. *Phys. Fluids* 18:Art. No. 012103 1–14
58. Martel C, Nicolas JA, Vega JM (1998) Surface-wave damping in a brimful circular cylinder. *J Fluid Mech* 360:213–228
59. Graham JMR (1980) The forces on sharp-edged cylinders in oscillatory flow at low Keulegan-Carpenter numbers. *J Fluid Mech* 97:331–346